Clinical characteristics and natural history of RHO-associated retinitis pigmentosa: a long-term follow-up study

Nguyen, X.T.A.; Talib, M.; Cauwenbergh, C. van; Schooneveld, M.J. van; Fiocco, M.; Wijnholds, J.; ... ; Boon, C.J.F.

SDC

OPEN

CLINICAL CHARACTERISTICS AND NATURAL HISTORY OF *RHO*-ASSOCIATED RETINITIS PIGMENTOSA

A Long-Term Follow-Up Study

XUAN-THANH-AN NGUYEN, MD,* MAYS TALIB, MD,* CAROLINE VAN CAUWENBERGH, PHD,† MARY J. VAN SCHOONEVELD, MD, PHD,‡ MARTA FIOCCO, PHD,§¶ JAN WIJNHOLDS, PHD,* JACOLINE B. TEN BRINK, BAS,** RALPH J. FLORIJN, PHD,** NICOLINE E. SCHALIJ-DELFOS, MD, PHD,* GISLIN DAGNELIE, PHD,†† MARIA M. VAN GENDEREN, MD, PHD,‡‡§§ ELFRIDE DE BAERE, MD, PHD,† MAGDA A. MEESTER-SMOOR, PHD,¶¶ JULIE DE ZAEYTIJD, MD,† IRINA BALIKOVA, MD, PHD,† ALBERTA A. THIADENS, MD, PHD,¶¶ CAREL B. HOYNG, MD, PHD,*** CAROLINE C. KLAVER, MD, PHD,¶¶***††† L. INGEBORGH VAN DEN BORN, MD, PHD,‡‡‡ ARTHUR A. BERGEN, PHD,**§§§ BART P. LEROY, MD, PHD,†¶¶¶ CAMIEL J.F. BOON, MD, PHD*‡

Purpose: To investigate the natural history of *RHO*-associated retinitis pigmentosa (RP).

Methods: A multicenter, medical chart review of 100 patients with autosomal dominant *RHO*-associated RP.

Results: Based on visual fields, time-to-event analysis revealed median ages of 52 and 79 years to reach low vision (central visual field $<20°$) and blindness (central visual field $<10°$), respectively. For the best-corrected visual acuity (BCVA), the median age to reach mild impairment ($20/67 \leq$ BCVA $<$ 20/40) was 72 years, whereas this could not be computed for lower acuities. Disease progression was significantly faster in patients with a generalized RP phenotype (n = 75; 75%) than that in patients with a sector RP phenotype (n = 25; 25%), in terms of decline rates of the BCVA ($P < 0.001$) and V4e retinal seeing areas ($P < 0.005$). The foveal thickness of the photoreceptor–retinal pigment epithelium (PR + RPE) complex correlated significantly with BCVA (Spearman's $\rho = 0.733$; $P < 0.001$).

Conclusion: Based on central visual fields, the optimal window of intervention for *RHO*-associated RP is before the 5th decade of life. Significant differences in disease progression are present between generalized and sector RP phenotypes. Our findings suggest that the PR + RPE complex is a potential surrogate endpoint for the BCVA in future studies.

RETINA 41:213–223, 2021

Mutations in the *RHO* gene are associated with the autosomal dominant form of retinitis pigmentosa (RP).[1] Initial symptoms of RP include night blindness or peripheral visual field (VF) loss, which can be followed by the loss of central vision in advanced stages of the disease. To date, more than 150 mutations in the *RHO* gene have been described, which are responsible for 25% to 30% of all autosomal dominant RP cases.[2] *RHO* mutations have also been described in congenital stationary night blindness[3] and, even more rarely, in forms of autosomal recessive RP.[4] Another phenotype commonly described in *RHO* mutations is sector RP, which is characterized by regional photoreceptor degeneration, typically confined to the inferior quadrant of the retina.[5,6] Sector RP is considered a stationary to slowly progressive disease but may eventually lead to a more severe, diffuse RP phenotype.[7]

The *RHO* gene encodes the protein rhodopsin, located in the outer segment of rod photoreceptor cells, containing extracellular, transmembrane, and cytoplasmic domains.[1] Previous studies have shown that the clinical expression of *RHO*-associated RP correlates with the protein domain affected by the mutation.[8] Mutations affecting the cytoplasmic domain of rhodopsin are more likely to cause a severe RP phenotype, with early loss of rod and cone function. By

contrast, patients with mutations affecting the extracellular domain generally have a milder phenotype, with relatively preserved rod and cone function and slower disease progression.[9,10]

No curative treatment for *RHO*-associated RP is currently available, but promising results have been achieved by knockdown and replacement gene therapy in animal models.[11,12] To guide the design of upcoming clinical trials, more insights into the natural disease progression in *RHO*-associated RP are necessary. A more detailed clinical disease profile will aid in the selection of eligible candidates and in the establishment of appropriate clinical endpoints for future trials. The purpose of this longitudinal study was to provide a description of the clinical variability and the natural disease course in patients with *RHO*-associated RP in a large cohort.

From the *Department of Ophthalmology, Leiden University Medical Center, Leiden, The Netherlands; †Department of Ophthalmology, Ghent University and Ghent University Hospital, Ghent, Belgium; ‡Department of Ophthalmology, Amsterdam UMC, Academic Medical Center, Amsterdam, The Netherlands; §Institute of Mathematic Leiden University, Leiden, The Netherlands; ¶Department of Biomedical Data Sciences, Leiden University Medical Center, Leiden, The Netherlands; **Department of Clinical Genetics, Amsterdam UMC, Academic Medical Center, Amsterdam, The Netherlands; ††Wilmer Eye Institute, Johns Hopkins University, Baltimore, Maryland; ‡‡Bartiméus, Diagnostic Centre for Complex Visual Disorders, Zeist, The Netherlands; §§Department of Ophthalmology, University Medical Center Utrecht, Utrecht, The Netherlands; ¶¶Department of Ophthalmology, Erasmus Medical Center, Rotterdam, The Netherlands; ***Department of Ophthalmology, Radboud University Medical Center, Nijmegen, The Netherlands; †††Department of Epidemiology, Erasmus Medical Center, Rotterdam, The Netherlands; ‡‡‡The Rotterdam Eye Hospital, Rotterdam, The Netherlands; §§§The Netherlands Institute for Neuroscience (NIN-KNAW), Amsterdam, The Netherlands; and ¶¶¶Ophthalmic Genetics & Visual Electrophysiology, Division of Ophthalmology, the Children's Hospital of Philadelphia, Philadelphia, Pennsylvania.

ERN-EYE is cofunded by the Health Program of the European Union under the Framework Partnership Agreement #739543—"ERN-EYE" and cofunded by the Hôpitaux Universitaires de Strasbourg.

None of the authors has any conflicting interests to disclose.

X.-T.-A. Nguyen and M. Talib are shared first authors.

Supplemental digital content is available for this article. Direct URL citations appear in the printed text and are provided in the HTML and PDF versions of this article on the journal's Web site (www.retinajournal.com).

This study was performed as part of a collaboration within the European Reference Network for Rare Eye Diseases (ERN-EYE).

Reprint requests: Camiel J.F. Boon, MD, PhD, Department of Ophthalmology, Leiden University Medical Center, Postal Zone J3-S, Albinusdreef 2, 2333 ZA Leiden, The Netherlands; e-mail: c.j.f.boon@lumc.nl

Materials and Methods

Study Population

Data of patients with *RHO*-associated RP were collected from the patient database for hereditary eye diseases (Delleman Archive) at the Amsterdam University Medical Center (the Netherlands) from various other Dutch tertiary referral centers within the RD5000 consortium[13] and from the Ghent University Hospital in Belgium. Inclusion criteria were as follows: a molecular confirmation of a (likely) pathogenic variant in the *RHO* gene or a first-degree relative with similar clinical findings and a molecular confirmation of a *RHO* mutation. In total, 100 patients with *RHO*-associated RP were included for analysis in this study. Approval from the ethics committee was obtained before the study as well as the local institutional review board approval in all participating centers. Dutch participants provided informed consent for the use of their patient data for research purposes. For Belgian participants, the local ethics committee waived the need for informed consent on the condition of pseudonymization.

Data Collection

A standardized review of medical records was performed for data on the initial symptoms, best-corrected visual acuity (BCVA), findings on slit-lamp examination and fundoscopy, Goldmann VFs, full-field electroretinogram (ERG), spectral-domain optical coherence tomography (SD-OCT), and fundus autofluorescence (FAF) imaging, where available. Goldmann VFs were digitized and converted to retinal seeing areas using methods previously described by Dagnelie.[14]

In patients with available OCT and FAF imaging in Heidelberg (Heidelberg Engineering, Heidelberg, Germany), automatic and manual measurements of retinal layers were performed using the inbuilt software of Heidelberg. The thickness of the photoreceptor–retinal pigment epithelium complex (PR + RPE) was defined as the foveal distance between the external limiting membrane and the basal border of the RPE, as described previously (see **Figure**, **Supplemental Digital Content 1**, http://links.lww.com/IAE/B219).[15] All measurements were performed by two authors (X.-T.-A.N. and M.T.) and reviewed by C.J.F. Boon in case of inconsistency between the aforementioned two authors.

Statistical Analysis

Data were analyzed using SPSS version 23.0 (IBM Corp, Armonk, NY) and the R software environment.[16]

Findings with a P value of < 0.05 were considered statistically significant. Normally and nonnormally distributed data were displayed as means with SDs and medians with interquartile ranges (IQRs), respectively. To measure the time to visual impairment, a time-to-event analysis was performed using the nonparametric maximum likelihood estimator method to account for left-censored, interval-censored, and right-censored data. Visual impairment endpoints were based on the criteria of the World Health Organization: no visual impairment (BCVA $\geq$ 20/40), mild visual impairment (20/67 $\leq$ BCVA $<$ 20/40), low vision (20/200 $\leq$ BCVA $<$ 20/67), severe visual impairment (20/400 $\leq$ BCVA $<$ 20/200), or blindness (BCVA $<$ 20/400). For VFs, the following endpoints were used: mild impairment (20° $\leq$ central VF $<$ 70°), low vision (central VF $<$ 20°), and blindness (central VF $<$ 10°). Because of the presence of repeated measurements, a linear mixed model analysis was performed to measure disease progression. For hand movement vision, light perception vision, and no light perception, logarithm of the minimum angle of resolution (logMAR) values of 2.7, 2.8, and 2.9 were used, respectively.[17] Structure–function correlations were analyzed using Spearman correlation coefficients. To analyze genotype–phenotype associations, patients were stratified into the following three groups based on the affected protein domain: cytoplasmic, transmembrane, or extracellular.

Results

Clinical and Genetic Characteristics

One hundred patients from 47 families, with autosomal dominant *RHO* mutations, were included from the Dutch (n = 63; 63%) and Belgian (n = 37; 37%) population. No differences in baseline characteristics between these two populations were present (see **Table**, **Supplemental Digital Content S2**, http://links.lww.com/IAE/B220). Patients with available longitudinal data (n = 72; 72%) had a median follow-up time of 6.9 years (IQR 11.9; range: 0.2–41.0) and a median of 5.0 visits (IQR 6.0; range: 2.0–31.0). Seventy-five patients (75%) had a generalized form of RP on fundus examination (Figure 1), whereas 25 patients (25%) showed a sector RP phenotype, with pigmentary changes confined to the inferior hemisphere in all cases. The clinical characteristics of the entire cohort are summarized in Table 1.

In total, 23 different missense mutations, 1 in-frame deletion, and 1 novel splice-site mutation were found in the *RHO* gene (see **Table**, **Supplemental Digital Content S3**, http://links.lww.com/IAE/B221). Patients were stratified, based on the affected protein domain, as carrying extracellular (n = 64; 64%), transmembrane (n = 20; 20%), or cytoplasmic (n = 15; 16%) mutations, excluding the splice-site mutation. We found a high proportion of extracellular mutations (24/25; 96%) in the sector RP group. The most common pathogenic variant in this study, p.(Glu181Lys), was found in four families, comprising 23 of the 63 Dutch patients (37%). This mutation was not found in the Belgian cohort. Common mutations exclusively found in the Belgian cohort were p.(Ile255del) (n = 6) and p.(Tyr178Asp) (n = 6), each belonging to a single family, accounting for 12 of the 37 Belgian patients (32%).

Visual Function

Best-corrected visual acuity data were available for 95 patients, with a high degree of symmetry between eyes (Spearman's $\rho = 0.888$; $P < 0.001$). In 25 patients, a degree of BCVA-based visual impairment was present during the last examination (see **Figure**, **Supplemental Digital Content 4**, http://links.lww.com/IAE/B222). Time-to-event analysis of the entire cohort revealed a median age of 72 years to reach mild visual impairment, whereas the median ages for low vision, severe visual impairment, and blindness could not be computed (Figure 2). First occurrences of low vision were seen from the 3rd decade of life onward, whereas severe visual impairment and blindness were seen from the 5th decade of life onward. In the sector RP cohort, the first occurrence of blindness was seen after the 8th decade of life in a patient with age-related macular degeneration. Linear mixed model analysis revealed an age effect on the mean BCVA, which was 0.012 logMAR (−2.9%; $P < 0.001$) per year for the entire cohort. The BCVA decline was significantly faster in patients with a generalized RP phenotype than that in patients with a sector RP phenotype ($P = 0.002$), with BCVA progression rates of 0.012 logMAR (−3.8%; $P < 0.001$) and −0.002 logMAR (+0.4%; $P = 0.671$) per year, respectively. For patients with generalized RP, we found no differences in baseline BCVA values ($P = 0.360$) or in progression slopes ($P = 0.168$) between affected protein domains.

Initial ERG findings were documented in 52 patients (Table 1). Minimal and nondetectable ERG responses were only found in the generalized RP group. The mean age at which nondetectable ERG responses were first observed was 35.3 years (SD 16.1; range 17.1–63.7). Longitudinal ERG data were available for 10 patients, with a mean follow-up time of 6.7 years (SD 4.0; range 0.5–13.6). Eight patients showed no clear changes in ERG patterns during follow-up.

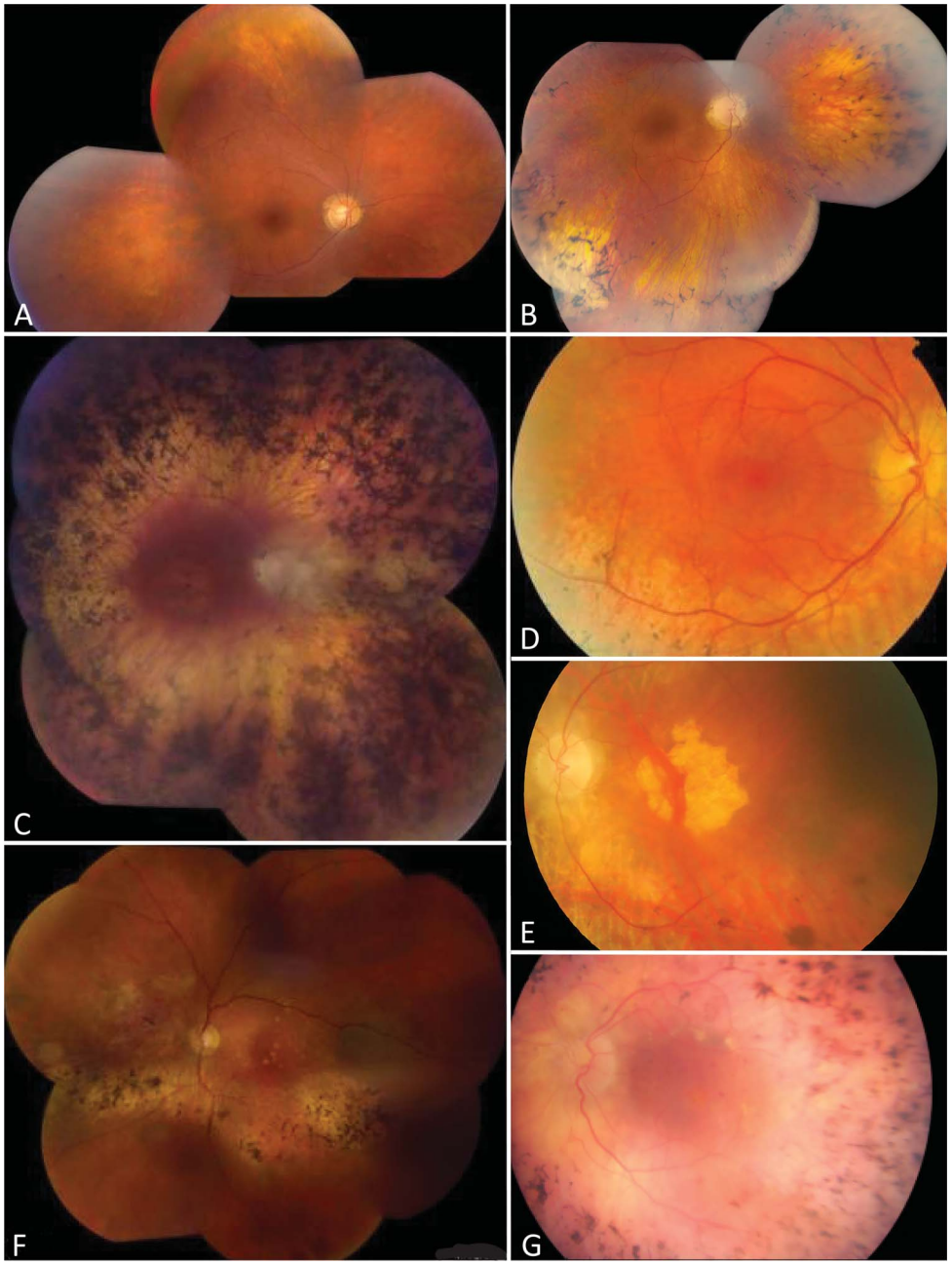

Fig. 1. Color fundus photography in this cohort of *RHO*-associated RP. **A–C.** Illustrations of interfamilial and intrafamilial variability fundus in a family with p.(Tyr178Asn) mutations in the *RHO* gene. **A.** Patient-ID 65, aged 38 years, with mutation p.(Tyr178Asn). Peripapillary atrophy and moderate peripheral chorioretinal atrophy was present on fundus photography. No intraretinal hyperpigmentation was seen (BCVA: 20/20 in both eyes). **B.** Patient-ID 66, aged 45 years, with *RHO* mutation p.(Tyr178-Asn). Fundus photography showed chorioretinal atrophy and bone-spicule hyperpigmentation in the midperiphery (BCVA right eye: 20/25; BCVA left eye: 20/67). **C.** Patient-ID 63, aged 50 years, carrying a p.(Tyr178Asn) in *RHO*. Fundus photography revealed optic disk pallor, attenuated vessels, ring-shaped atrophy in the macula, and diffuse intraretinal bone-spicule hyperpigmentations (BCVA was 20/400 in both eyes). **D.** Patient-ID 52, aged 45 years, with *RHO* mutation p.(Glu28His). A sectorial RP phenotype is seen on color fundus photography of the right eye, with peripapillary atrophy and atrophic areas and bone-spicule hyperpigmentation around the inferior vascular arcade (BCVA: 20/20 in both eyes). **E.** Patient-ID 51, aged 87 years, with *RHO* mutation p.(Leu40Pro). Fundus photography showed mild optic disk pallor with retinal atrophy following the superior and inferior vascular arcade. Geographic atrophy is visible at the macula of the left eye, resulting in a BCVA of only light perception. **F.** Patient-ID 80, aged 74 years, carrying a p.(Asn15Ser) mutation in *RHO*. Fundus photography of the left eye revealed paravascular atrophy mainly in the inferior quadrant with the pigment clumping around these atrophic areas. Drusen can be seen around the macula (BCVA right eye: 20/22; BCVA left eye: 20/67). **G.** Patient-ID 48, aged 74 years, with the p.(Asp190Gly) *RHO* mutation, showing advanced RP. A pale fundus with a waxy pale optic disk, severely attenuated vessels, CME, and bone-spicule hyperpigmentation in the midperipheral retina (BCVA right eye: 20/667; BCVA left eye: 20/1,000).

Two patients, aged 29 and 26 years, displayed rod–cone patterns at the initial visit, which progressed to minimal and absent responses over a time span of 8.6 and 13.6 years, respectively.

Original Goldmann VF records were available for 59 patients, with a high degree of symmetry between eyes for the V4e (Spearman's $\rho = 0.957$; $P < 0.001$) and the I4e (Spearman's $\rho = 0.935$; $P < 0.001$) retinal seeing areas. Various patterns of VF defects were observed, ranging from mild concentric constriction to central islands (Figure 3). Intrafamilial variability was present, as patients carrying the p.(Glu181Lys) mutation could demonstrate different VF defects (Figure 3, A and B). Time-to-event analysis of the VFs revealed median ages of 44, 52, and 79 years for mild visual impairment, low vision, and blindness, respectively (Figure 1B). For the

Table 1. Characteristics of Patients With *RHO*-Associated (Sector) RP at the Last Examination

Characteristics	Total (n = 100)	Generalized RP (n = 75)	Sector RP (n = 25)	*P*
Male (%)	44 (44)	34 (46)	10 (39)	0.642
Age at the last examination (n = 100)				
Mean ± SD	43.5 ± 18.5	42.5 ± 19.3	45.5 ± 22.6	0.204
Initial symptoms (n = 55)				
Nyctalopia, n (%)	41 (75)	28 (74)	2 (40)	
VF loss, n (%)	5 (9)	3 (8)	1 (20)	
Visual acuity loss, n (%)	3 (5)	2 (5)	1 (20)	
Multiple symptoms, n (%)	6 (11)	5 (13)	1 (20)	0.890*
Age at onset in years (n = 55)				
Early childhood, n (%)	21 (38)	16 (29)	5 (9)	
Median age (IQR)	13.5 (12.5)	11.0 (11.8)	15.7 (12.5)	0.829
Mean refractive error, in D (n = 66)				
Mean ± SD	0.8 ± 2.85	1.0 ± 3.27	0.2 ± 1.4	0.298
BCVA in the better-seeing eye (n = 95)				
Median BCVA, in Snellen (IQR)	20/25 (20/30)	20/30 (20/30)	20/20 (20/200)	**<0.001**
BCVA in the worst-seeing eye (n = 95)				
Median BCVA, in Snellen (IQR)	20/30 (20/25)	20/33 (20/30)	20/22 (20/60)	**0.002**
ERG patterns (n = 52)				
Normal responses, n (%)	2 (4)	—	2 (11)	
Reduced responses, n (%)†	5 (10)	1 (3)	4 (22)	
Rod–cone patterns, n (%)	28 (54)	16 (47)	12 (67)	
Minimal responses, n (%)	6 (11)	6 (18)	—	
Nondetectable, n (%)	11 (21)	11 (32)	—	**<0.001***
Retinal seeing areas, V4e (n = 57)‡				
Median seeing areas, in mm^2 (IQR)	256.4 (545.6)	128.0 (552.4)	487.2 (248.3)	0.067
Retinal seeing areas, I4e (n = 55)‡				
Median seeing areas, in mm^2 (IQR)	17.4 (101.4)	14.5 (66.5)	130.6 (194.36)	**0.011**
VF patterns (n = 75)				
Normal, n (%)	1 (1)	1 (2)	—	
Peripheral constriction, n (%)	24 (32)	19 (32)	5 (31)	
Midperipheral scotoma, n (%)	6 (8)	5 (9)	1 (6)	
Central island with peripheral remnants, n (%)	18 (24)	15 (25)	3 (19)	
Central preservation, n (%)	19 (25)	18 (30)	1 (6)	
Superior hemisphere, n (%)	7 (10)	1 (2)	6 (38)	**0.002***
CME, n (%)	16/32 (50)	14/25 (56)	2/7 (29)	0.225*
Central retinal thickness (n = 32)‡				
Median thickness in μm (IQR)	253.0 (94.0)	254.0 (122.0)	248.5 (92.5)	0.858
Outer nuclear layer thickness (n = 32)‡				
Median thickness in μm (IQR)	97.5 (47.25)	89.5 (52.5)	110.5 (41.9)	0.121
PR + RPE thickness (n = 32)‡				
Median thickness in μm (IQR)	90.5 (18.3)	89.5 (20.0)	95.3 (18.1)	0.147
EZ bandwidth (n = 26)‡				
Mean width in μm ± SD	2,704.5 ± 1881.9	2,125.0 ± 1,544.8	4,277.5 ± 1909.6	**0.007**
Hyper-AF ring diameter (n = 15)‡				
Horizontal border in μm ± SD	3,541.6 ± 1930.6	3,484.9 ± 2058.5	3,910.3 ± 1,009.4	0.571
Vertical border in μm ± SD	2,652.7 ± 1,567.7	2,594.9 ± 1,628.0	3,201.5 ± 883.2	0.286

Significant *P* values ($P < 0.05$) are indicated in bold. The last available examination was used for documentation.
*Fisher's exact test was performed.
†No clear rod or cone response was documented.
‡Averaged between eyes.
D, diopters.

V4e retinal seeing areas, a faster decline of retinal seeing areas was observed in patients with generalized RP than in patients with sector RP ($P = 0.005$), with a significant decline rate of -5.6% per year ($P < 0.001$) for patients with generalized RP, but not in patients with sector RP (+1.7% per year, $P = 0.477$). No differences in V4e retinal seeing areas were seen between domains at baseline ($P = 0.240$) nor with increasing age ($P = 0.085$) in patients with generalized RP. For the I4e retinal seeing areas, we found the age effect to be

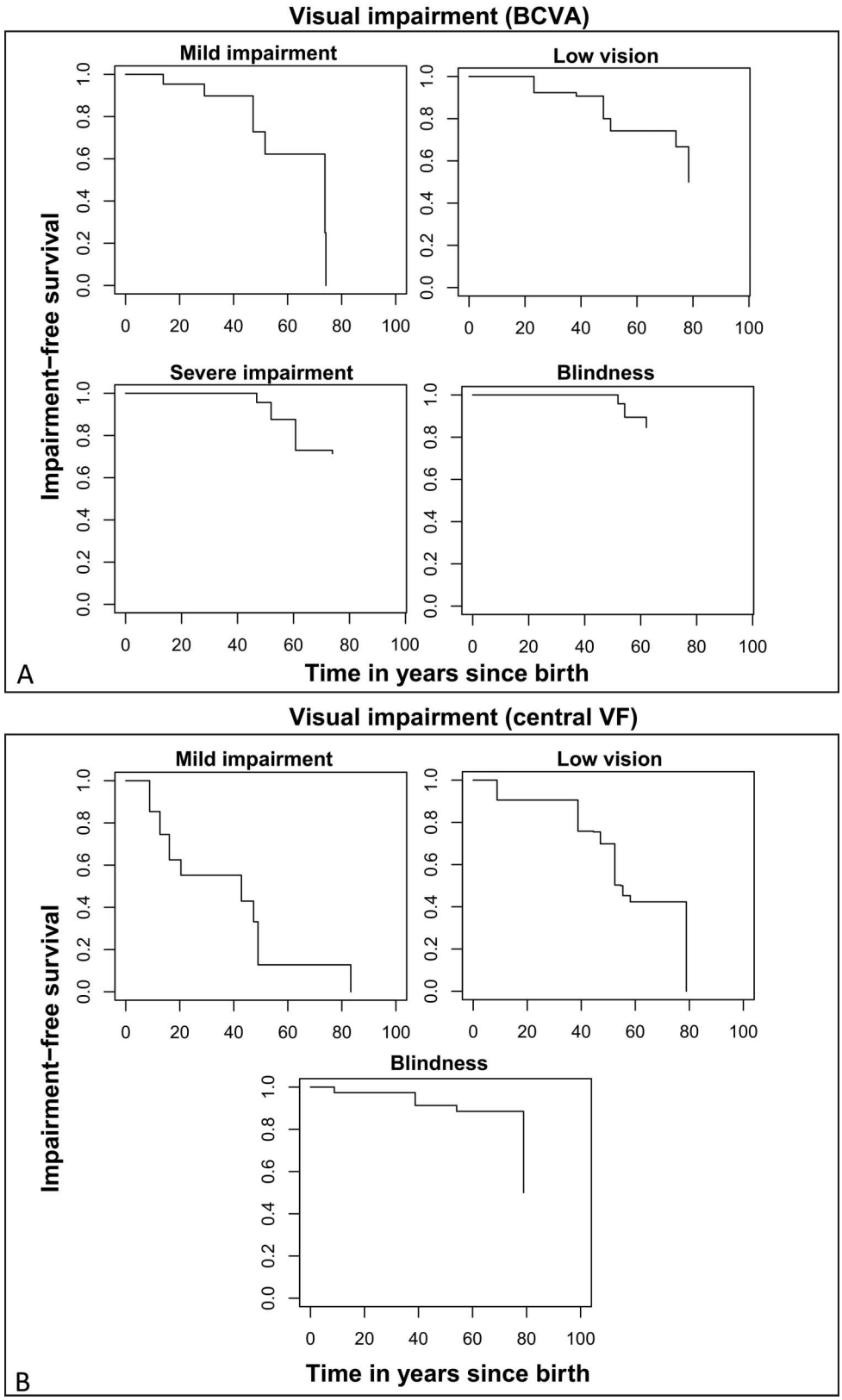

Fig. 2. Time-to-event analysis illustrating the time to reach visual impairment based on the definition set by the World Health Organization. Because of the presence of left-censored, interval-censored, and right-censored data to estimate the time to reach low vision, severe impairment, and blindness, the nonparametric maximum likelihood estimator was used. **A.** Time-to-event analysis of the BCVA in the better-seeing eye demonstrating the time to reach mild visual impairment [(20/67 ≤ BCVA < 20/40), low vision (20/200 ≤ BCVA < 20/67), severe visual impairment (20/400 ≤ BCVA < 20/200), or blindness (BCVA < 20/400). **B.** For central VFs, the following endpoints were used: mild impairment (20° ≤ central VF < 70°), low vision (central VF < 20°), and blindness (central VF < 10°).

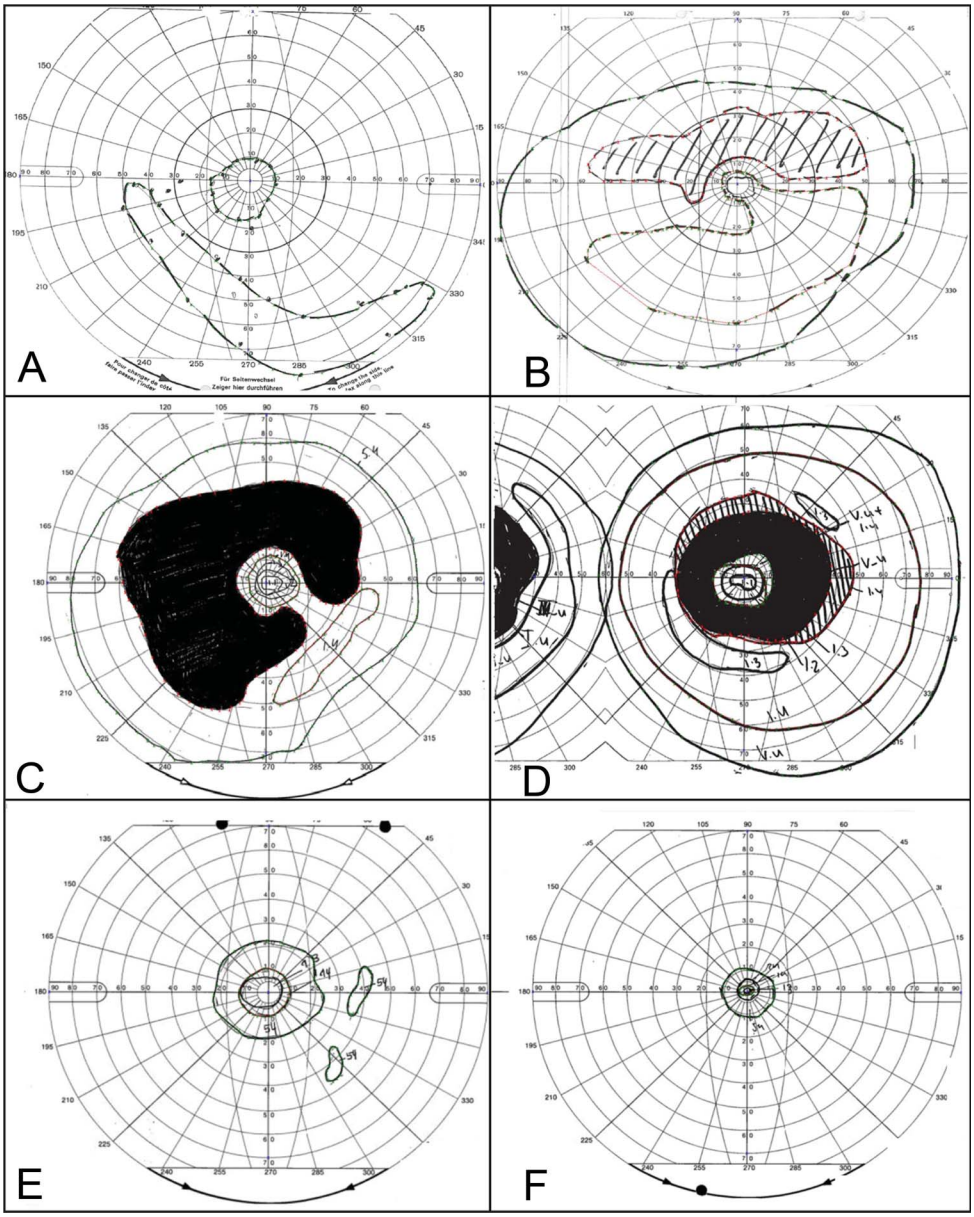

Fig. 3. Representative patterns of VF loss in patients with *RHO*-associated RP. **A** and **B.** Intrafamilial variability in a family carrying the p.(Glu181Lys) mutation. **A.** Patient-ID 30, aged 54 years, showed a central island with peripheral remnants (BCVA right eye: 20/100; BCVA left eye: 20/125) on kinetic perimetry, whereas the younger brother (**B**), aged 46 years, had an absolute scotoma in the superior hemifield (BCVA: 20/16 in both eyes). **C.** Patient-ID 52, aged 43 years, with the *RHO* missense mutation p.(Glu28His). An incomplete midperipheral annular scotoma was visible in the left eye (BCVA right eye: 20/25; BCVA left eye: 20/20). **D.** Patient-ID 39, aged 52 years, with a c.937-2A>C [p.(?)] splice-site mutation in *RHO*, showing a complete ring scotoma in the right eye (BCVA right eye: 20/67; BCVA left eye: 20/400). **E.** Patient-ID 59, aged 22 years, with *RHO* mutation p.(Arg135Trp), showing severe constriction of the V4e and I4e isopters with central preservation of the VF and small midperipheral VF remnants (BCVA right eye: 20/67; BCVA left eye: 20/40). **F.** Patient-ID 44 (38 years of age), carrying the p.(Asp190Tyr) *RHO* mutation, had marked peripheral VF loss with only a residual central island remaining (BCVA right eye: 20/50; BCVA left eye: 20/32).

−5.5% per year ($P < 0.001$) in patients with generalized RP and +0.2% per year ($P = 0.930$) in patients with sector RP. For patients with generalized RP, we found differences at baseline ($P = 0.013$), with larger I4e retinal seeing areas in patients with extracellular mutations than those in patients with transmembrane ($P = 0.005$) or cytoplasmic ($P = 0.026$) mutations. No differences in progression slopes of I4e retinal seeing areas were observed between affected domains ($P = 0.233$).

Multimodal Imaging

Spectral-domain OCT imaging was performed in 32 patients, with thickness measurements of retinal layers specified in Table 1. We found cystoid macular edema (CME) in 16 of the 32 patients (50%), which was located in the fovea for 12 of the 16 (75%) patients. No significant age effect was found on central retinal thickness ($P = 0.371$) or outer nuclear layer thickness ($P = 0.502$), after exclusion of patients with foveal CME. For PR + RPE measurements, advancing age was associated with the loss of PR + RPE thickness (−0.6% per yr; $P = 0.030$), which was not affected by a sector RP phenotype ($P = 0.611$). The PR + RPE thickness was the only parameter, after exclusion of patients with foveal CME and correction for multiple testing, that correlated with the BCVA (Table 2). The macular ellipsoid zone (EZ) bandwidth, measurable in

Table 2. Structure and Function Correlations in *RHO*-Associated RP

	BCVA (logMAR)		Seeing Retinal Area V4e		Seeing Retinal Area I4e	
Visual Function Parameter	Spearman's rho	*P*	Spearman's rho	*P*	Spearman's rho	*P*
SD-OCT imaging						
CRT*	−0.370	0.095	0.291	0.274	0.086	0.770
ONL thickness*	−0.234	0.366	−0.029	0.923	−0.162	0.596
PR + RPE thickness*	−0.733	**<0.001**	0.528	0.053	0.556	0.049
EZ bandwidth	−0.506	0.054	0.198	0.517	0.280	0.379
FAF imaging						
Horizontal ring diameter	−0.339	0.235	0.632	0.024	0.643	0.021
Vertical ring diameter	−0.245	0.419	0.615	0.037	0.566	0.059

The most recent mean values between right and left eyes were used for analysis. Imaging and measurements were performed using the Heidelberg inbuilt software (Spectralis SD-OCT + HRA, Heidelberg Engineering, Heidelberg, Germany). The significance level was set at 0.003 after Bonferroni correction. Significant values are in bold.

*Patients with CME located in the fovea were excluded from analysis.

CRT, central retinal thickness; ONL, outer nuclear layer.

26 of the 32 (81%) patients, decreased with advancing age (−3.8%; $P < 0.001$), which was not significantly different in patients with sector RP ($P = 0.589$). However, a larger EZ bandwidth at baseline was seen in patients with a sector RP phenotype ($P = 0.018$). For patients with generalized RP, no differences in the EZ bandwidth at baseline ($P = 0.185$) or for the decline rates ($P = 0.886$) were observed between affected protein domains. In 6 of the 26 patients (23%), the EZ bandwidth went beyond the scanning range on SD-OCT (Figure 4A). A granular interrupted aspect of the EZ bandwidth was seen in 9 of the 26 (35%) patients.

Fundus AF imaging, available for 38 patients, revealed hyperautofluorescent (hyper-AF) and hypoautofluorescent (hypo-AF) patterns in variable degrees, including a hyper-AF macular ring in 26 of the 38 (68%) patients (Figure 4). In patients with sector RP, a common pattern seen on FAF was a hypo-AF distribution along the inferior vascular arcade, which corresponded with areas of degeneration seen on fundus photography (Figure 4D). A high degree of correlation was found between EZ bandwidth and the horizontal ($\rho = 0.923$; $P < 0.001$) and vertical borders ($\rho = 0.937$; $P < 0.001$) of the hyper-AF macular ring.

Discussion

This multicenter study provides a detailed description of the natural history of *RHO*-associated autosomal dominant RP, using cross-sectional and longitudinal data. We found a high prevalence of the p.(Gly181Lys) mutation (n = 23) in four different families, accounting for 37% of the Dutch cohort. This mutation has rarely been described in other populations, which is suggestive of a founder effect of p.(Gly181Lys) in the Dutch *RHO*-associated autosomal dominant patients. Common mutations exclusively found in the Belgian patients of our cohort were p.(Ile255del) and p.(Tyr178Asp). The p.(Tyr178Asp) mutation has never been described outside the Belgian population,[18] whereas the p.(Ile255del) mutation has previously been found in a single Irish family.[19]

Several mutations, such as p.(Glu181Lys), found in this cohort could present as either generalized or sector RP, which underlines the potential influence of genetic and/or other modifiers on the phenotype. As suggested previously, it is possible that sector RP will eventually transition into a generalized RP phenotype in later stages of the disease.[7] However, we were not able to observe this transition in any of our patients. In addition, we found patients who retained a sector RP phenotype up to the 8th decade of life.

Our reported progression rates of the BCVA (−3.8% per yr) and V4e retinal seeing areas (−5.6% per yr) in patients with generalized RP were faster than those reported by a previous natural history study on *RHO*-associated RP, which reported rates of −1.8% per year for the BCVA and −2.6% per year for V4e retinal seeing areas.[9] One possible explanation for this discrepancy is the difference in statistical methods. In contrast to the study of Berson et al,[9] we analyzed patients with sector RP separately because these patients demonstrated minimal disease progression and may contribute to a ceiling effect. In addition, there are notable genetic differences between our population and the one in the American study by Berson et al. The p.(Pro23His) mutation, which is the most common *RHO* mutation in the United States (36% in their cohort), is known to express a particularly mild phenotype and is also described in patients with sector RP.[20] To the best of our knowledge, this founder mutation has never been reported in European studies, including the present one.[21,22]

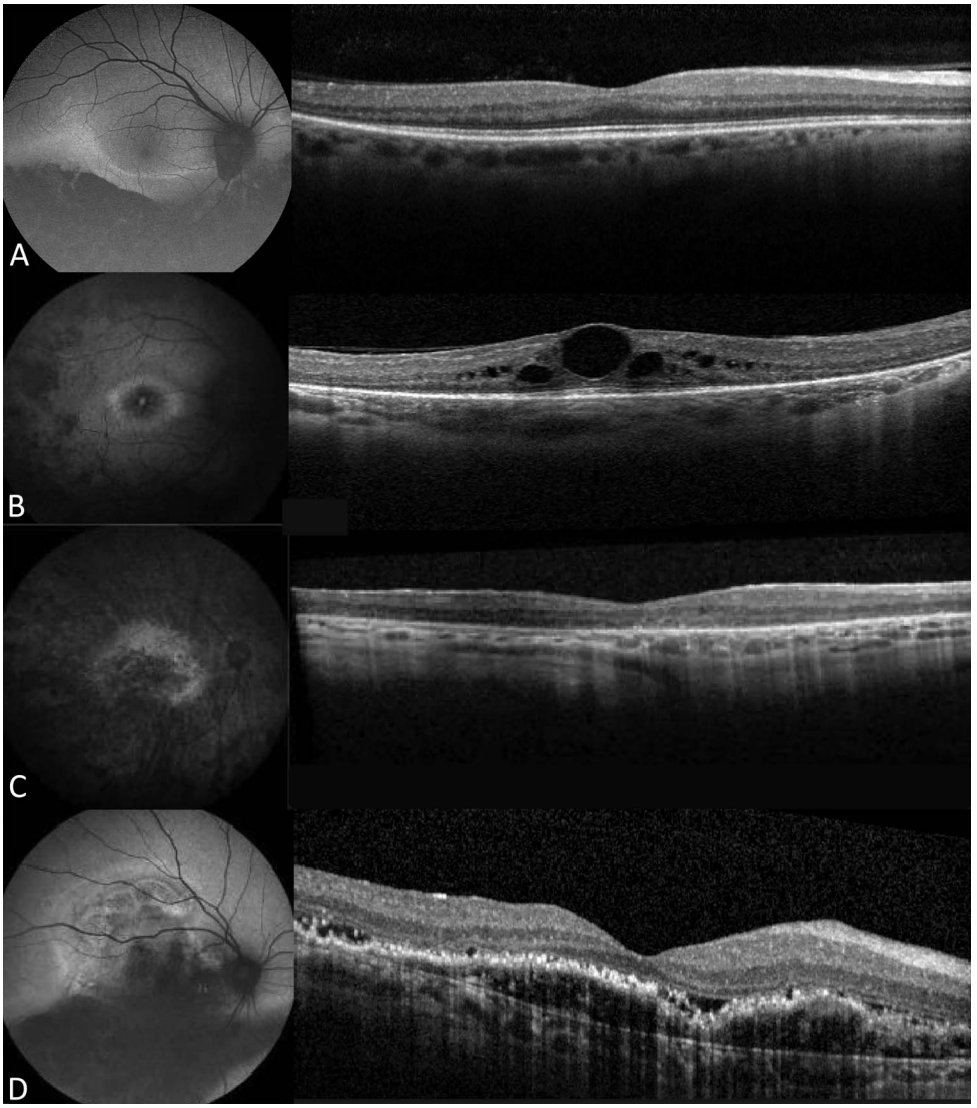

Fig. 4. Fundus AF and corresponding SD-OCT imaging in patients with *RHO*-associated RP. **A.** Patient-ID 81, aged 47 years, carrying the missense mutation p.(Asn15Ser). Fundus AF imaging showed an inferior sectoral hypo-AF and ERG responses were reduced in a rod–cone pattern. Spectral-domain OCT imaging in this patient revealed central preservation of outer retinal layers but with thinning of these layers in the peripheral macula. The EZ bandwidth went beyond the scanning range nasally (BCVA right eye: 20/20; BCVA left eye: 20/22). **B.** Patient-ID 70, aged 26 years, with a p.(Glu181Lys) missense mutation. A well-demarcated hyper-AF ring was visible on FAF, with hypo-AF regions inside the hyper-AF ring. A small hyper-AF spot was seen at the foveal site, corresponding to the site of CME on SD-OCT. The midperipheral retina displayed normal AF regions surrounded by granular hypo-AF in variable intensities. Cystoid fluid collections were present in the inner and outer nuclear layer (BCVA right eye: 20/28; BCVA left eye: 20/33). **C.** Patient-ID 88, aged 60 years, carrying a p.(Pro347Leu) missense mutation in the *RHO* gene. Fundus AF imaging reveals the near absence of AF in the fovea and midperipheral retina, with residual AF remaining in the posterior pole. No evident hyper-AF ring is seen. Profound atrophy of all retinal layers is present on SD-OCT, with increased visibility of the underlying choroidal vessels. Granular remnants of the EZ are seen at the central fovea, but the EZ is completely absent in the peripheral macula (BCVA was 20/400 in both eyes). **D.** Patient-ID 80, aged 74 years, carrying the *RHO* missense mutation p.(Asn15Ser). Fundus AF imaging showed sectorial degeneration hypo-AF along the inferior vascular arcade, corresponding with the RPE atrophy seen on fundus photography (Fig. 1F). On SD-OCT, a pigment epithelial detachment was observed. The partly hyperreflective structures underlying the RPE detachment suggest the presence of a neovascular membrane. The different layers of the neuroretina were still discernible, with a BCVA of 20/33 and 20/22 in the right and left eye, respectively.

Patients with a generalized form of RP were stratified based on the domains affected by *RHO* mutations. At baseline, we found larger EZ bandwidths on OCT and I4e retinal seeing areas on Goldmann VF in patients carrying extracellular mutations than in patients with transmembrane or cytoplasmic mutations. No differences in annual decline rates of EZ bandwidths and I4e retinal seeing areas were found between mutated protein domains. In addition, mutations causing sector RP, showing minimal disease progression, were predominantly found in the extracellular domains. These findings support previous research in suggesting that extracellular mutations cause milder phenotypes in *RHO*-associated RP.[23–25] The differences in disease expression between affected domains can be attributed to the biochemical defects caused by the mutations within these domains, although external modifiers such as increased light exposure, especially in the development of sector RP, may also play a role.[2,7]

A limitation of this study is its retrospective nature, which limited a complete ascertainment of clinical data. Electroretinogram data were not available for all patients and were mainly performed at baseline for

diagnostic purposes. For this reason, a previously used classification system could not be applied to this cohort.[10,23,24] A prospective standardized natural history study on *RHO*-associated RP, which is currently unavailable to the best of our knowledge, should be able to address such limitations.

Preclinical studies on several gene knockdown and replacement strategies for *RHO*-associated RP have shown promising results, paving the way for human gene therapy trials.[11,12] Our current clinical findings can have significant implications for future clinical treatment trials. We found a high degree of between-eye symmetry for all visual parameters (BCVA, V4e, and I4e seeing retinal areas), supporting the use of the fellow eye as a control in intervention studies. On SD-OCT imaging, we found a high prevalence of CME, which may be a concern for future gene therapy trials because the presence of CME may alter the retinal morphology, challenging correct injection of viral vectors into the subretinal space and posing additional risks for preoperative and postoperative complications.[26] The borders of the hyper-AF ring on FAF imaging, which demarcates the transition zone between the affected and unaffected retina,[27] correlated strongly with the EZ bandwidth. Fundus AF imaging should be used in conjunction with SD-OCT to capture disease progression in less advanced stages of *RHO*-associated RP, in which the EZ bandwidth can go beyond the 30° scanning range of SD-OCT (occurring in 23% of our cases).

The optimal intervention window for *RHO*-associated RP is before the 5th decade of life because time-to-event analysis of VFs revealed median ages of 52 and 79 years for low vision and blindness, respectively. The use of the visual acuity as an endpoint may be impractical for *RHO*-associated RP because of the relatively late onset of BCVA-based impairment. Therefore, the use of surrogate endpoints for the visual acuity could accelerate the measurement of disease progression and treatment response. We and others have previously found that the PR + RPE complex has been suggested to be a good predictor of the visual acuity.[15,28–30] Similar results were found in this study because the PR + RPE complex correlated strongly with the BCVA, and it was the only parameter that remained significant after correction for multiple testing. The PR + RPE complex can potentially be used to identify early structural changes before the visual acuity loss may be noticeable, which can be particularly useful in diseases with relatively slow disease progression such as *RHO*-associated RP. In anticipation of future clinical trials for *RHO*, the establishment of potential clinical endpoints is a necessary step for an optimal study design. In this regard, this study highlights the potential use of the PR + RPE complex as a surrogate endpoint for the BCVA in future clinical trials.

Key words: inherited retinal dystrophies, natural history, retinitis pigmentosa, rhodopsin, sector retinitis pigmentosa.

References

1. Dryja TP, Hahn LB, Cowley GS, et al. Mutation spectrum of the rhodopsin gene among patients with autosomal dominant retinitis pigmentosa. Proc Natl Acad Sci U S A 1991;88:9370–9374.
2. Verbakel SK, van Huet RAC, Boon CJF, et al. Non-syndromic retinitis pigmentosa. Prog Retin Eye Res 2018;66:157–186.
3. Zeitz C, Gross AK, Leifert D, et al. Identification and functional characterization of a novel rhodopsin mutation associated with autosomal dominant CSNB. Invest Ophthalmol Vis Sci 2008;49:4105–4114.
4. Comitato A, Di Salvo MT, Turchiano G, et al. Dominant and recessive mutations in rhodopsin activate different cell death pathways. Hum Mol Genet 2016;25:2801–2812.
5. Kranich H, Bartkowski S, Denton MJ, et al. Autosomal dominant "sector" retinitis pigmentosa due to a point mutation predicting an Asn-15-Ser substitution of rhodopsin. Hum Mol Genet 1993;2:813–814.
6. Berson EL, Rosner B, Sandberg MA, et al. Ocular findings in patients with autosomal dominant retinitis pigmentosa and a rhodopsin gene defect (pro-23-his). Arch Ophthalmol 1991;109:92–101.
7. Ramon E, Cordomí A, Aguilà M, et al. Differential light-induced responses in sectorial inherited retinal degeneration. J Biol Chem 2014;289:35918–35928.
8. Iannaccone A, Man D, Waseem N, et al. Retinitis pigmentosa associated with rhodopsin mutations: correlation between phenotypic variability and molecular effects. Vis Res 2006;46:4556–4567.
9. Berson EL, Rosner B, Weigel-DiFranco C, et al. Disease progression in patients with dominant retinitis pigmentosa and rhodopsin mutations. Invest Ophthalmol Vis Sci 2002;43:3027–3036.
10. Mendes HF, van der Spuy J, Chapple JP, et al. Mechanisms of cell death in rhodopsin retinitis pigmentosa: implications for therapy. Trends Mol Med 2005;11:177–185.
11. Tsai YT, Wu WH, Lee TT, et al. Clustered regularly interspaced short palindromic repeats-based genome surgery for the treatment of autosomal dominant retinitis pigmentosa. Ophthalmology 2018;125:1421–1430.
12. Cideciyan AV, Sudharsan R, Dufour VL, et al. Mutation-independent rhodopsin gene therapy by knockdown and replacement with a single AAV vector. Proc Natl Acad Sci 2018;115:E8547.
13. van Huet RAC, Oomen CJ, Plomp AS, et al. The RD5000 Database: facilitating clinical, genetic, and therapeutic studies on inherited retinal diseases. Invest Ophthalmol Vis Sci 2014;55:7355–7360.
14. Dagnelie G. Technical note. Conversion of planimetric visual field data into solid angles and retinal areas. Clin Vis Sci 1990;5:95–100.
15. Spaide RF, Curcio CA. Anatomical correlates to the bands seen in the outer retina by optical coherence tomography: literature review and model. Retina 2011;31:1609–1619.

16. R: A Language and Environment for Statistical Computing [computer Program]. Vienna, Austria: R Foundation for Statistical Computing; 2010.
17. Talib M, van Schooneveld MJ, Thiadens AA, et al. Clinical and genetic characteristics of male patients with RPGR-Associated retinal dystrophies: a long-term follow-up study. Retina 2019;39:1186–1199.
18. Van Cauwenbergh C, Coppieters F, Roels D, et al. Mutations in splicing factor genes are a major cause of autosomal dominant retinitis pigmentosa in Belgian families. PLoS One 2017; 12:e0170038.
19. Inglehearn CF, Bashir R, Lester DH, et al. A 3-bp deletion in the rhodopsin gene in a family with autosomal dominant retinitis pigmentosa. Am J Hum Genet 1991;48:26–30.
20. Oh KT, Weleber RG, Lotery A, et al. Description of a new mutation in rhodopsin, pro23ala, and comparison with electroretinographic and clinical characteristics of the pro23his mutation. Arch Ophthalmol 2000;118:1269–1276.
21. Blanco-Kelly F, García-Hoyos M, Cortón M, et al. Genotyping microarray: mutation screening in Spanish families with autosomal dominant retinitis pigmentosa. Mol Vis 2012;18:1478–1483.
22. Audo I, Manes G, Mohand-Saïd S, et al. Spectrum of rhodopsin mutations in French autosomal dominant rod-cone dystrophy patients. Invest Ophthalmol Vis Sci 2010;51:3687–3700.
23. Cideciyan AV, Hood DC, Huang Y, et al. Disease sequence from mutant rhodopsin allele to rod and cone photoreceptor degeneration in man. Proc Natl Acad Sci U S A 1998;95: 7103–7108.
24. Jacobson SG, McGuigan DB, Sumaroka A, et al. Complexity of the class B phenotype in autosomal dominant retinitis pigmentosa due to rhodopsin mutations. Invest Ophthalmol Vis Sci 2016;57:4847–4858.
25. Schuster A, Weisschuh N, Jägle H, et al. Novel rhodopsin mutations and genotype-phenotype correlation in patients with autosomal dominant retinitis pigmentosa. Br J Ophthalmol 2005;89:1258.
26. Xue K, Groppe M, Salvetti AP, et al. Technique of retinal gene therapy: delivery of viral vector into the subretinal space. Eye 2017;31:1308–1316.
27. Aizawa S, Mitamura Y, Hagiwara A, et al. Changes of fundus autofluorescence, photoreceptor inner and outer segment junction line, and visual function in patients with retinitis pigmentosa. Clin Exp Ophthalmol 2010;38:597–604.
28. Eliwa TF, Hussein MA, Zaki MA, et al. Outer retinal layer thickness as good visual predictor in patients with diabetic macular edema. Retina 2018;38:805–811.
29. Lim JI, Tan O, Fawzi AA, et al. A pilot study of Fourier-domain optical coherence tomography of retinal dystrophy patients. Am J Ophthalmol 2008;146:417–426.
30. Talib M, van Schooneveld MJ, Van Cauwenbergh C, et al. The spectrum of structural and functional abnormalities in female carriers of pathogenic variants in the RPGR gene. Invest Ophthalmol Vis Sci 2018;59:4123–4133.